Biochimica et Biophysica Acta 1827 (2013) 1112–1122

Contents lists available at SciVerse ScienceDirect

Biochimica et Biophysica Acta

journal homepage: www.elsevier.com/locate/bbabio

Review

Nitrogenase assembly ☆

Yilin Hu *, Markus W. Ribbe *

Department of Molecular Biology and Biochemistry, University of California, Irvine, CA 92687-3900, USA

ARTICLE INFO

Article history:
Received 17 October 2012
Received in revised form 2 December 2012
Accepted 3 December 2012
Available online 8 December 2012

Keywords:
Nitrogenase
Metallocluster
Assembly
P-cluster
M-cluster

ABSTRACT

Nitrogenase contains two unique metalloclusters: the P-cluster and the M-cluster. The assembly processes of P- and M-clusters are arguably the most complicated processes in bioinorganic chemistry. There is considerable interest in decoding the biosynthetic mechanisms of the P- and M-clusters, because these clusters are not only biologically important, but also chemically unprecedented. Understanding the assembly mechanisms of these unique metalloclusters is crucial for understanding the structure–function relationship of nitrogenase. Here, we review the recent advances in this research area, with an emphasis on our work that provide important insights into the biosynthetic pathways of these high-nuclearity metal centers. This article is part of a Special Issue entitled: Metals in Bioenergetics and Biomimetics Systems.

1. Introduction

Nitrogenase plays a key role in global nitrogen cycle. Harbored in a group of microorganisms called diazotrophs, nitrogenase is capable of catalyzing the reduction of atmospheric dinitrogen (N_2) to bioavailable ammonia (NH_3) in a nucleotide-dependent process [1,2]. The overall reaction catalyzed by nitrogenase is usually depicted as $N_2 + 8H^+ + 8e^- + 16ATP \rightarrow 2NH_3 + H_2 + 16ADP + 16P_i$. The ability of nitrogenase to break the inert N≡N triple bond under ambient conditions not only enables the production of an ample supply of "fixed" nitrogen through a mild biological process, but also makes nitrogenase a fascinating subject from the perspective of chemical energy. As such, nitrogenase has remained a topic of intense research for decades.

Three homologous nitrogenases, namely, the molybdenum (Mo), vanadium (V) and iron (Fe)-only nitrogenases, have been identified [3]. Among them, the best studied is the Mo nitrogenase of *Azotobacter vinelandii*, which consists of (i) the Fe protein (or NifH), a γ_2-dimer that contains a $[Fe_4S_4]$ cluster between the two subunits and one ATP binding site within each subunit; and (ii) the MoFe protein (or NifDK), an $\alpha_2\beta_2$-tetramer that contains two complex metallocenters per αβ-subunit pair: a P-cluster ($[Fe_8S_7]$) at each α/β-subunit interface and an M-cluster ($[MoFe_7S_9C$-homocitrate$]$) within each α-subunit [4–7]. Upon substrate turnover, the two component proteins of Mo nitrogenase form a functional complex [8], which facilitates the inter-protein transfer of electrons in the sequence of $[Fe_4S_4]$ cluster (NifH) → P-cluster (NifDK) → M-cluster (NifDK) and the subsequent reduction of substrates at the M-cluster site (Fig. 1). The P- and M-clusters are intriguing from a chemical point of view, as both are high-nuclearity metalloclusters that have evaded successful chemical synthesis so far. Moreover, these clusters are biologically important, as their unique structural and redox properties underlie the distinctive reactivity of nitrogenase.

The P-cluster mediates the electron flow from NifH to NifDK. Bridged between the α- and β-subunits of NifDK, it is located 10 Å below the surface of the protein [4,5]. Structurally, the P-cluster can be viewed as two $[Fe_4S_3]$ partial cubanes bridged by a μ_6-sulfide in between (Fig. 2A and B). In the presence of excess dithionite, the P-cluster exists in an all-ferrous, diamagnetic state (designated the P^N state). Upon treatment of a dye oxidant [*e.g.*, indigodisulfonate (IDS)], the P^N state can be two-electron oxidized to a stable S = integer (3 or 4) state (designated the P^{OX} state), which displays a characteristic, parallel-mode EPR[1] signal at $g = 11.8$ [9–11]. In both P^N and P^{OX} states (Fig. 2A and B), the P-cluster is covalently coordinated to NifDK by six cysteinyl ligands: three from the α-subunit ($Cys^{\alpha62}$, $Cys^{\alpha88}$ and $Cys^{\alpha154}$) and three from the β-subunit ($Cys^{\beta70}$, $Cys^{\beta95}$ and $Cys^{\beta153}$). Both the P^N and P^{OX} structures have each of the $Cys^{\alpha62}$, $Cys^{\alpha154}$, $Cys^{\beta70}$ and $Cys^{\beta153}$ ligands ligate to one Fe atom, and each of the $Cys^{\alpha88}$ and $Cys^{\beta95}$ residues ligate to two Fe atoms

Abbreviations: EPR, electron paramagnetic resonance; MCD, magnetic circular dichroism; XAS, x-ray absorption spectroscopy; EXAFS, extended x-ray absorption fine structure; SAXS, small angle x-ray scattering; HPLC, high performance liquid chromatography; MS, mass spectrometry; ATP, adenosine triphosphate; ADP, adenosine diphosphate; MoO_4^{2-}, molybdate; IDS, indigo disulfonate; SAM, *S*-adenosyl-methionine; SAH, *S*-adenosyl-homocysteine; 5'-dA, 5′-deoxyadenosine

☆ This article is part of a Special Issue entitled: Metals in Bioenergetics and Biomimetics Systems.

* Tel.: +1 949 824 9509; fax: +1 949 824 8551.
E-mail addresses: yilinh@uci.edu (Y. Hu), mribbe@uci.edu (M.W. Ribbe).

[1] See refs. [59,60] for EPR and XAS spectroscopy of metalloproteins.

0005-2728/$ – see front matter © 2012 Elsevier B.V. All rights reserved.
http://dx.doi.org/10.1016/j.bbabio.2012.12.001

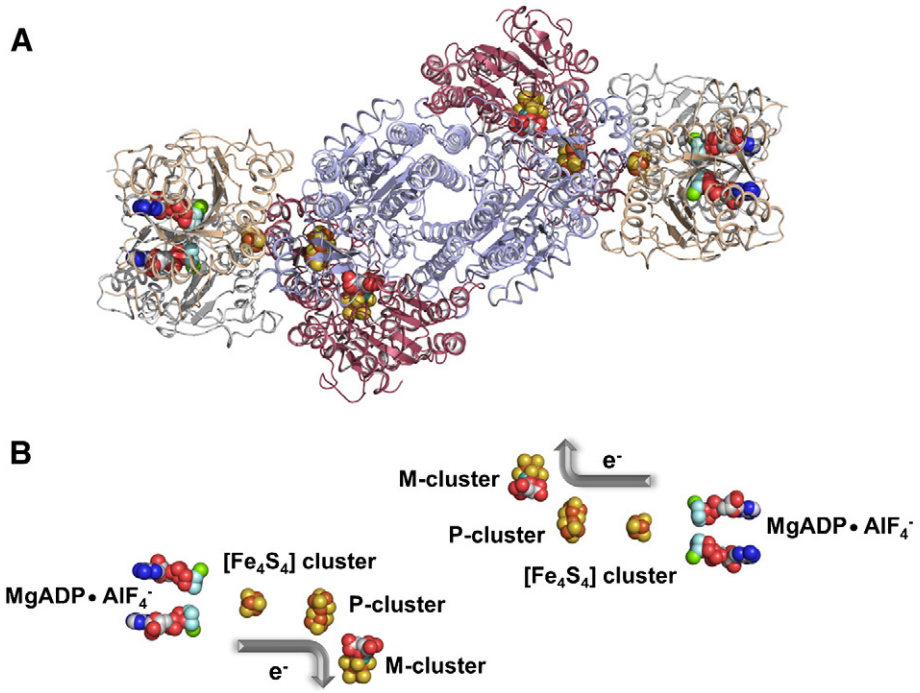

Fig. 1. Crystal structure of the ADP•AlF_4^--stabilized NifH/NifDK complex (A) and the relative positions of components involved in the electron flow (B). The two γ-subunits of NifH are colored gray and light brown, and the α- and β-subunits of NifDK are colored red and light blue, respectively. All clusters and ADP•AlF_4^- are shown as space-filling models. Atoms are colored as follows: Fe, orange; S, yellow; Mo, cyan; O, red; C, gray; N, dark blue; Mg, green; Al, beige; F, light blue. PYMOL was used to create the figure (PDB ID: 1N2C).

[5,12,13]. However, the two oxidation states of the P-cluster do differ in their core structures, with one half of the P^{OX} state in a more open conformation (Fig. 2B). Such a rearrangement in cluster structure is further accompanied by changes in the ligation between the cluster and the protein [13]. Compared to the P^N state, the P^{OX} state is coordinated by two additional protein ligands: $Ser^{\beta188}$, which coordinates an Fe atom through an Oγ ligand along with the cysteinyl group of $Cys^{\beta153}$; and $Cys^{\alpha88}$, which coordinates an Fe atom through a backbone amide N ligand and a cysteinyl group (Fig. 2B).

The M-cluster serves as the active site for substrate reduction. Buried within the α-subunit of NifDK, it is located 14 Å away from the P-cluster. Structurally, the M-cluster can be viewed as [Fe_4S_3] and [$MoFe_3S_3$] partial cubanes bridged by three μ_2-sulfides in between (Fig. 2C). It also contains a homocitrate moiety at the Mo end and a μ_6-interstitial carbide in the center [4–7,14–16]. The M-cluster is coordinated to NifDK by only two ligands: $Cys^{\alpha275}$, which ligates the apical Fe atom; and $His^{\alpha442}$, which ligates the opposite Mo atom. In addition, $Lys^{\alpha426}$ provides an anchor for the homocitrate moiety [4]. The "simple" coordination pattern of M-cluster facilitates the extraction of this cluster as an intact entity into organic solvents, such as N-methylformamide (NMF). Both protein-bound and solvent-isolated M-clusters display a characteristic, $S = 3/2$ EPR signal at $g =$ 4.7, 3.7 and 2.0 in the presence of excess dithionite, although the signal of the isolated M-cluster is broader in line-shape than the signal of its protein-bound counterpart [14,17]. The M-cluster can undergo a reversible one-electron redox process, which is visualized by a change in the intensity of the $S = 3/2$ signal [1]. The core charge of the M-cluster was proposed to be +1 or +3 in the resting state [18,19]; however, the isolated M-cluster was shown to be anionic [14]. Such an overall negative charge of the M-cluster is believed to originate from its homocitrate entity, which is −4 upon deprotonation of the –OH group.

The assembly processes of P- and M-clusters are arguably the most complex processes in bioinorganic chemistry. Understanding the assembly mechanisms of these unique metalloclusters is crucial for understanding the structure–function relationship of nitrogenase.

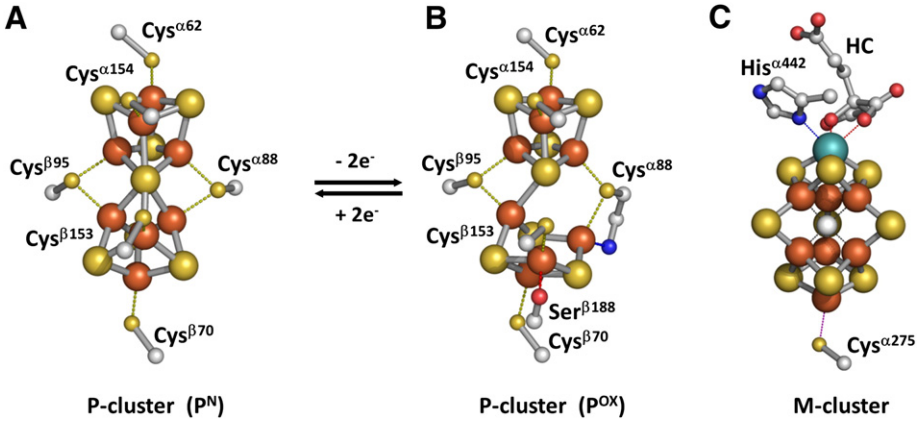

Fig. 2. Crystal structures of the P^N (A) and P^{OX} (B) states of the P-cluster and the M-cluster (C). The clusters are shown as ball-and-stick models, with the atoms colored as described in the legend of Fig. 1. PYMOL was used to create the figure (PDB IDs: 1M1N and 3MIN). HC, homocitrate.

Here, we review the recent advances in this research area, with an emphasis on our work that provide important insights into the biosynthetic pathways of P- and M-clusters. An alternative view of some aspects of M-cluster assembly can be found elsewhere [20].

2. P-cluster assembly

The P-cluster is assembled at its target location in NifDK (hence the term "*in situ*" assembly). This process involves the reductive coupling of a pair of $[Fe_4S_4]$-like clusters—one at a time—at the two α/β-subunit interfaces of NifDK (Section 2.1), which in turn coordinates the stepwise assembly of the two αβ-halves of NifDK (Section 2.2).

2.1. Reductive coupling of $[Fe_4S_4]$-like clusters into an $[Fe_8S_7]$ P-cluster

The geometric symmetry of P-cluster has led to the proposal that this 8Fe cluster is assembled through the fusion of two 4Fe subclusters. This hypothesis was supported indirectly by the earlier recovery of $[Fe_4S_4]$ fragments from P-cluster extraction attempts [2], as well as the recent success in chemically synthesizing P-cluster topologs from 4Fe precursors [21–27]. The direct biological proof for this theory, however, came from the characterization of two NifDK variants of *A. vinelandii*: one, designated Δ*nifB* NifDK, was isolated from a *nifB*-deletion background; the other, designated Δ*nifH* NifDK, was isolated from a *nifH*-deletion background. Both Δ*nifB* NifDK and Δ*nifH* NifDK are M-cluster-deficient, as NifB and NifH are two essential protein factors for M-cluster biosynthesis (see Section 3). However, Δ*nifB* NifDK contains a normal P-cluster, displaying, in the IDS-oxidized state, a $g = 11.8$ parallel-mode signal that is characteristic of the P^{OX} state; whereas Δ*nifH* NifDK contains an unusual "P-cluster", displaying, in the dithionite-reduced state, an $S = 1/2$ EPR signal that is characteristic of $[Fe_4S_4]^{1+}$ clusters [28]. Fe K-edge XAS/EXAFS analyses (footnote 1) reveal that the "P-cluster" in Δ*nifH* NifDK (designated P*-cluster) consists of a pair of un-bridged $[Fe_4S_4]$-like clusters [29,30]: one of them has the standard $[Fe_4S_4]$ architecture; whereas the other is distorted (*i.e.*, with a bridging Cys replacing a core sulfide) and/or coordinated by a light atom (*e.g.*, N or O from Asp, His, Ser or adventitious water) (Fig. 3A). MCD analysis provides further support for the EXAFS-derived model of the P*-cluster, showing that this cluster is composed of a ferredoxin-type, $[Fe_4S_4]^{1+}$ cluster and a diamagnetic, $[Fe_4S_4]$-like cluster [31,32].

The P*-cluster in Δ*nifH* NifDK can be converted, *in vitro*, to a mature P-cluster, upon incubation with NifH, MgATP and dithionite [30]. Such a transformation is reflected by the disappearance of the P*-specific, $S = 1/2$ signal and the concomitant appearance of the P^{OX}-specific, $g = 11.8$ signal [30]. Moreover, it is consistent with the EXAFS-based observation of elongated/altered Fe–S/Fe–Fe backscattering distances [30]. These observations firmly establish the P*-cluster as the physiologically-relevant precursor to P-cluster. The two 4Fe units of P*-cluster are likely supplied by NifS and NifU, with

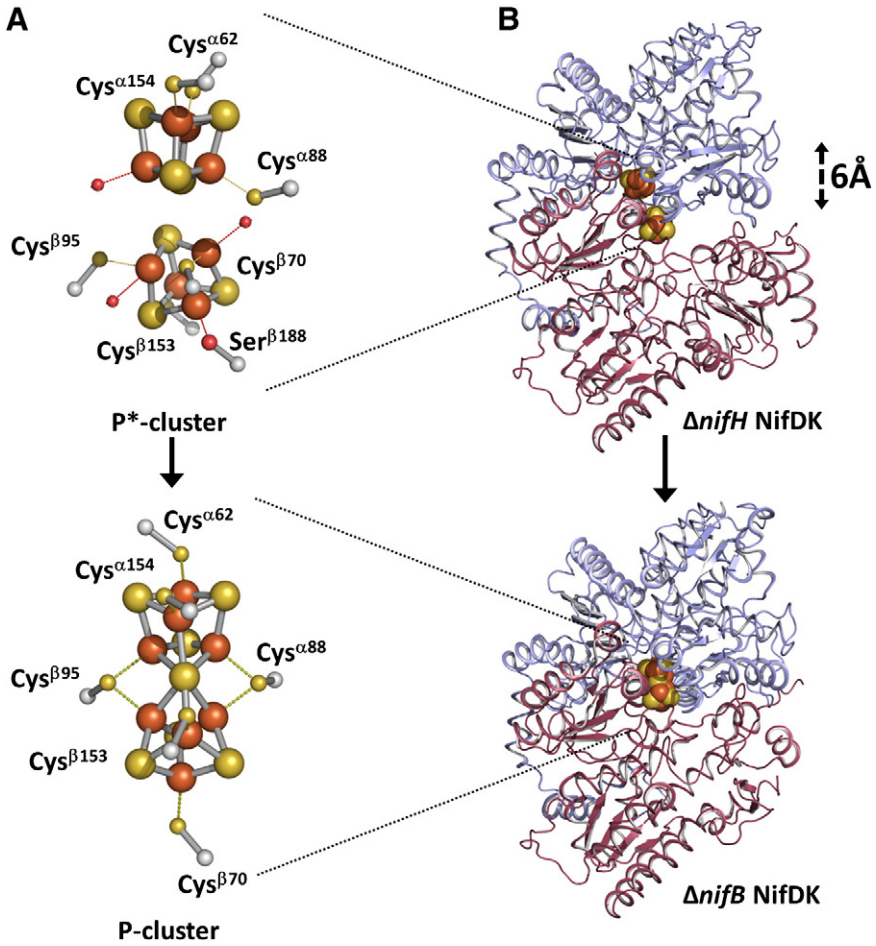

Fig. 3. Coupling of a pair of $[Fe_4S_4]$-like clusters (designated P*-cluster) into a mature $[Fe_8S_7]$ P-cluster (A) and the concomitant conformational change of NifDK at the α/β-subunit interface (B). (A) The P*-cluster comprises one standard $[Fe_4S_4]$ cubane (top) and one $[Fe_4S_4]$-like fragment that is distorted and/or coordinated by additional light atoms (bottom), which can be reductively coupled into a $[Fe_8S_7]$ structure upon incubation with NifH, MgATP, and dithionite. The clusters are shown as ball-and-stick models. (B) Ribbon diagrams of the αβ-dimers of P*-cluster-containing Δ*nifH* NifDK (top) and P-cluster-containing Δ*nifB* NifDK (bottom). The diagram on top represents the best model of Δ*nifH* NifDK based on SAXS data [34], which was constructed from the structure of the wild-type NifDK by deletion of the M-cluster, followed by a symmetric 6 Å-translation of the α- and β-subunits about the *y* axis. The subunits and atoms are colored as described in the legend of Fig. 1. PYMOL was used to create the figure (PDB IDs: 1M1N and 1L5H).

NifS (a pyridoxal phosphate-dependent cysteine desulfurase) forming a protein-bound cysteine persulfide that is subsequently donated to NifU for the sequential formation of [Fe_2S_2] and [Fe_4S_4] clusters [33]. The *in vitro* maturation of P*-cluster can be maximized at certain concentrations of reductant (dithionite) and reductase (NifH), suggesting that redox chemistry plays a crucial role in this process [30]. XAS analyses demonstrate that the Fe atoms of the clusters undergo successive reduction upon maturation till they eventually stabilize at a near all-ferrous oxidation state [30], further illustrating that this process involves the reductive coupling of two 4Fe units into an 8Fe entity. The chemical details of this process are yet to be defined; however, it was reported recently that an [Fe_8S_7] core could be synthesized chemically from two all-ferric [Fe_4S_4] clusters *via* phosphine desulfurization [27]. This observation suggests a plausible mechanism of P-cluster maturation that involves the reductive desulfurization of an [Fe_4S_4] cluster.

The strict dependence of P-cluster maturation on ATP hydrolysis points to a second role of NifH in the capacity of an ATP-dependent reductase, one that is critical for the assembly of nitrogenase. NifH may act in a similar manner in assembly and catalysis, both of which involve the docking of NifH on NifDK, the conformational rearrangement of the two proteins, and the electron transfer from the former to the latter; only in the case of P-cluster assembly, NifH is specifically required for the redox-tuning and the proper positioning of the [Fe_4S_4]-like clusters for efficient coupling. Consistent with this hypothesis, comparative SAXS analysis shows that Δ*nifH* NifDK exists in a more extended conformation ($R_g = 45.7$ Å) than Δ*nifB* NifDK ($R_g = 42.4$ Å) [34]. The increase in the overall size of Δ*nifH* NifDK correlates with an increase in the solvent accessibility of the Fe atoms of the P-cluster species, which can be best modeled by a 6 Å gap at the α/β-subunit interface (Fig. 3B, *upper*) that is absent from the structure of Δ*nifB* NifDK (Fig. 3B, *lower*). Thus, NifH may bring the α- and β-subunits of NifDK in closer proximity, thereby facilitating the coupling of the two [Fe_4S_4]-like clusters while providing added stability to the α/β-subunit interface of NifDK.

2.2. Stepwise assembly of the two P-clusters in the two αβ-halves of NifDK

The two P-clusters in NifDK are not matured simultaneously; rather, they are formed one at a time, concomitant with the stepwise assembly of the two αβ-halves of NifDK. The first indication of such a stepwise mechanism came from the capture of a NifDK variant with half P-cluster content. Designated Δ*nifB*Δ*nifZ* NifDK, this NifDK species was Isolated from a *nifB*/*nifZ*-deletion background of *A. vinelandii* [35]. Biochemical and MCD analyses indicate that Δ*nifB*Δ*nifZ* NifDK contains a fully assembled P-cluster in one αβ-dimer pair and a P*-cluster-like precursor in the other αβ-dimer [35,36]. Consistent with this suggestion, Δ*nifB*Δ*nifZ* NifDK displays both the P*-specific $S = 1/2$ signal (in the dithionite-reduced state) and the P^{OX}-specific $g = 11.8$ parallel-mode signal (in the IDS-oxidized state); however, the former signal is ~50% in intensity relative to the signal of Δ*nifH* NifDK (containing two P*-clusters), while the latter signal is ~50% in intensity relative to the signal of Δ*nifB* NifDK (containing two P-clusters) (Fig. 4B, C). Thus, Δ*nifH* NifDK, Δ*nifB*Δ*nifZ* NifDK and Δ*nifB* NifDK represent three sequential snapshots of P-cluster assembly. Maturation of the "second" P*-cluster in Δ*nifB*Δ*nifZ* NifDK, like that of the P*-clusters in Δ*nifH* NifDK, requires NifH, MgATP and

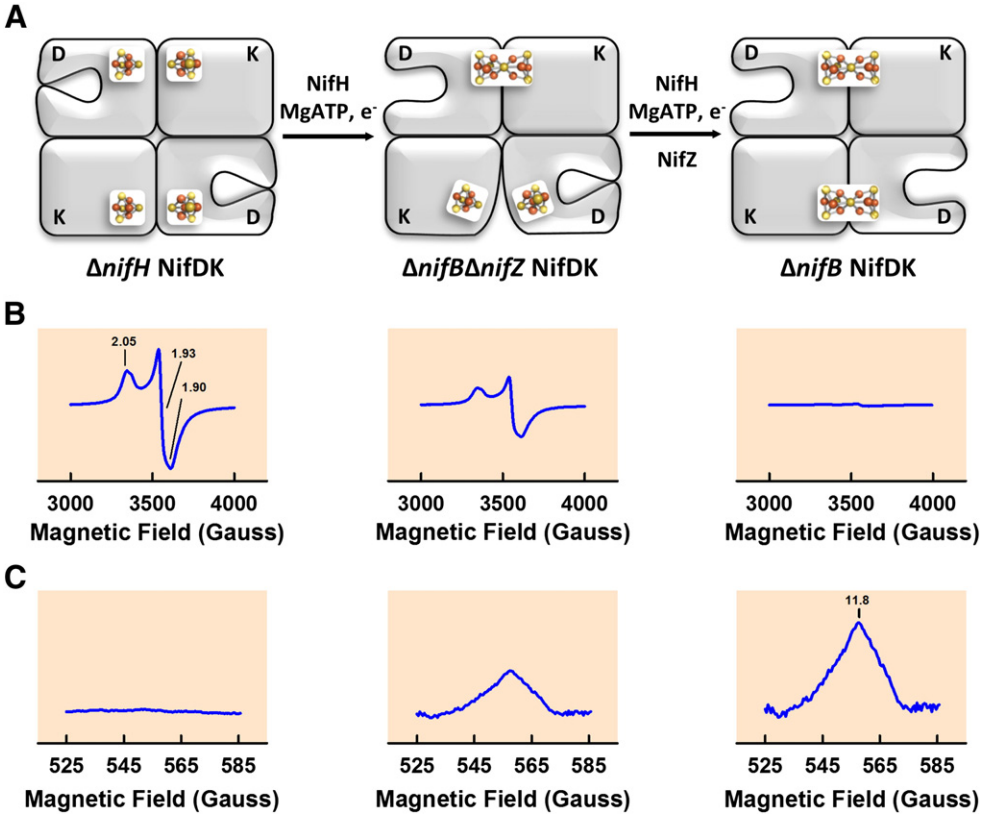

Fig. 4. Stepwise assembly of P-clusters in NifDK (A) and EPR features of the assembly intermediates in the dithionite-reduced (B) and IDS-oxidized (C) states. (A) The different conformations of P-cluster during assembly are represented by Δ*nifH* NifDK (left), which contains two [Fe_4S_4] cluster pairs (or P*-clusters); Δ*nifB*Δ*nifZ* NifDK (middle), which contains one P-cluster and one [Fe_4S_4] cluster pair (or P*-cluster); and Δ*nifB* NifDK (right), which contains two P-clusters. Maturation of the "first" P-cluster requires NifH, whereas maturation of the "second" P-cluster requires both NifH and NifZ. Formation of the P-cluster at the α/β-subunit interface also induces a conformational change of the α-subunit, which "opens" up the M-cluster site. (B and C) The P*-cluster in Δ*nifH* NifDK (B, left) displays a characteristic $S = 1/2$ signal at $g = 2.05$, 1.93, and 1.90 in the dithionite-reduced state; the P-cluster in Δ*nifB* NifDK (C, right) displays a characteristic $g = 11.8$ parallel-mode signal in the IDS-oxidized state; the Δ*nifB*Δ*nifZ* NifDK (B and C, middle) displays both P*- and P-specific signals at ~50% intensity.

dithionite; however, it also requires an additional protein factor, NifZ. Although the exact function of NifZ is unclear, it could modify some key residues at the second α/β-subunit interface, which is specifically required for the coupling of the second [Fe_4S_4] pair [35,37].

Interestingly, the permanent conformation of Δ*nifB*Δ*nifZ* NifDK can be captured transiently during the maturation process of the P-clusters in Δ*nifH* NifDK. Upon incubation of Δ*nifH* NifDK with NifH, MgATP and dithionite, there is an increase in the magnitude of the P^{OX}-specific signal, which aligns well with the increase in the activity of the protein [30]. Both show a "lag" period at approximately 50% of their respective maximum values, and both match well with the maturation of the second P-cluster in Δ*nifB*Δ*nifZ* NifDK in the post-lag phases. Consistent with the biphasic changes in the spectroscopic feature and enzymatic activity of Δ*nifH* NifDK, the shift of Fe K-edge energy is unevenly paced, and EXAFS fits further demonstrate a change in the ratio of short to long Fe–Fe distance in two distinct steps, suggesting a biphasic change in the redox state (*i.e.*, Fe K-edge energy) and structural arrangement (*i.e.*, Fe–Fe distance) of the cluster during maturation [30]. Together, these observations provide dynamic proofs of a stepwise assembly mechanism of the P-clusters in NifDK, with the conformation at the lag phase representing the completion of P-cluster assembly in the first αβ-dimer of the protein. It should be noted that maturation of both P-clusters in Δ*nifH* NifDK only requires the action of NifH, likely due to the fact that the protein is expressed in a *nifZ*-intact background and, therefore, has already "seen" the action of NifZ [30].

The unsynchronized assembly events of P-clusters render a stepwise maturation pattern of the two αβ-halves of NifDK. Apart from providing stability to the α/β-subunit interface, the assembly of P-cluster also impacts the conformation of the M-cluster binding site within the α-subunit of NifDK. Prior to the maturation of P-clusters, the M-cluster sites in Δ*nifH* NifDK assume a "closed" conformation that does not allow the access of M-cluster (Fig. 4A). Upon P-cluster maturation, however, the M-cluster sites are "opened up" and assume the same conformation as that of the M-cluster sites in Δ*nifB* NifDK (Fig. 4A) [38]. Thus, the assembly of P-cluster is not an isolated event; rather, it "prepares" the binding site for M-cluster insertion, the last step of M-cluster assembly (see Section 3 below). NifH plays a pivotal in these processes, serving as an ATP-dependent reductase while inducing conformational changes of NifDK for both P-cluster maturation and M-cluster insertion.

3. M-cluster assembly

M-cluster is assembled outside its target location in NifDK (hence the term "*ex situ*" assembly). Arguably one of the most complex processes in bioinorganic chemistry, the biosynthesis of M-cluster requires, minimally, the participation of *nifS*, *nifU*, *nifB*, *nifE*, *nifN*, *nifV* and *nifH* gene products. This process involves the formation of an Fe/S core (Section 3.1), the insertion of Mo and homocitrate (Section 3.2), and the transfer of M-cluster to its final binding site (Section 3.3).

3.1. Formation of an Fe/S core

The Fe/S core of M-cluster is formed on NifB and subsequently delivered to NifEN (Fig. 5A and B). It has been proposed that NifS and NifU are responsible for supplying [Fe_4S_4] clusters to NifB, where they are processed into a large Fe/S core that contains all Fe and S necessary for the generation of a mature M-cluster [39]. Consistent with this proposal, deletion of *nifB* results in the accumulation of a NifDK species that is deficient in M-cluster (see discussion of Δ*nifB* NifDK in Section 2 above), suggesting an indispensible function of NifB in

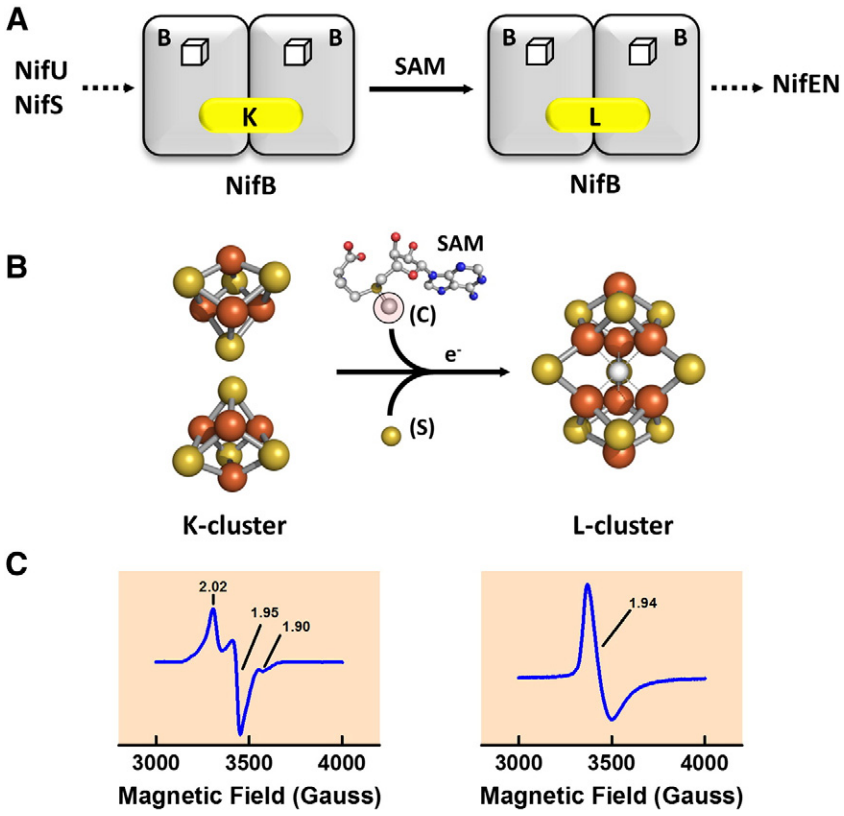

Fig. 5. Schematic presentation (A), structural details (B) and the accompanying spectral changes (C) of the formation of L-cluster on NifB. (A and B) NifS and NifU supply [Fe_4S_4] clusters to NifB, which forms an [Fe_8S_9] L-cluster through the coupling of the two [Fe_4S_4] modules of K-cluster concomitant with the insertion of a sulfur atom and a carbon atom in a radical SAM-dependent process. The L-cluster is subsequently transferred to NifEN. The clusters and SAM are shown as ball-and-stick models, with the atoms colored as described in the legend of Fig. 1. PYMOL was used to create the figure (PDB ID: 3PDI). (C) The K-cluster and SAM-cluster collectively give rise to a SAM-responsive, $S = 1/2$ signal at $g = 2.02$, 1.95 and 1.90 in the dithionite-reduced state (left); whereas the L-cluster displays a characteristic $g = 1.94$ signal in the IDS-oxidized state (right).

M-cluster assembly [38]. Sequence analysis reveals that NifB has a conserved CxxxCxxC signature motif at its N terminus, which is characteristic of a family of radical *S*-adenosyl-L-methionine (SAM)-dependent enzymes. In addition, NifB contains sufficient ligands for the coordination of the entire complement of the Fe atoms of M-cluster [40]. These observations suggest that the formation of an Fe/S core on NifB may follow a novel synthetic route that relies on the radical chemistry at its SAM domain. In one plausible scenario, NifB could bridge two $[Fe_4S_4]$ units (supplied by NifU) concomitant with the insertion of an S atom and a C atom *via* a SAM-dependent mechanism.

Support for this hypothesis came from the characterization of a NifEN-B fusion protein. This fusion protein was generated by fusing the *nifN* and *nifB* genes together and expressing the fused genes homologously in a *nifHDK*-deletion background of *A. vinelandii* [41]. The resultant fusion protein represents an "integrated" assembly unit comprising two adjacent components along the biosynthetic pathway of M-cluster. Two cluster species are accumulated on NifEN-B: one, designated the K-cluster, consists of a pair of $[Fe_4S_4]$ clusters; the other, designated the L-cluster, is a $[Fe_8S_9]$ cluster (Fig. 5B). Identification of the K-cluster is facilitated by the observation of a distinctive $S = 1/2$ signal ($g = 2.02$, 1.95 and 1.90) that is associated with the NifB entity of the fusion protein (Fig. 5C, *left*). Upon addition of SAM, this $S = 1/2$ signal disappears concomitant with the appearance of an L-cluster-specific $g = 1.94$ signal (Fig. 5C, *right*), suggesting the coupling of two 4Fe clusters (*i.e.*, the K-cluster) into an 8Fe cluster (*i.e.*, the L-cluster) [41]. Initially identified on NifEN alone, the L-cluster represents an all-Fe homolog to M-cluster that is transferred from NifB to NifEN upon completion of synthesis [42–45]. Fe K-edge XAS and crystallographic analyses show that it closely resembles the core structure of M-cluster, except for the replacement of Fe by Mo/homocitrate at one end of the cluster (Fig. 5B). Biochemical analysis further demonstrates the physiological relevance of this cluster, showing that it can be matured into an M-cluster upon incorporation of Mo and homocitrate (see Section 3.2 below). Together, these observations confirm the function of NifB in synthesizing a large Fe/S core (L-cluster) from smaller Fe/S fragments (K-cluster) in a SAM-dependent manner.

Further insights into the role of radical SAM chemistry in this process were acquired through the analysis of the pattern of SAM cleavage by NifEN-B [46]. HPLC and MS analyses show that SAM is cleaved by NifEN-B into 5'-deoxyadenosine (5'-dA) and *S*-adenosyl-homocysteine (SAH) (Fig. 6A). Deuterium labeling experiments further demonstrate that incubation of NifEN-B with [methyl-d_3]-SAM (where the three hydrogen atoms of the methyl group of SAM are labeled with deuterium) results in the formation of deuterium-enriched 5′-dA. Interestingly, the same SAM cleavage pattern was observed in the cases of RlmN and Cfr, two radical SAM-dependent, RNA methylating enzymes [47,48]. The mechanism of these enzymes has been proposed to involve (i) the transfer of methyl group from one equivalent of SAM (leaving SAH behind); (ii) the generation of 5′-dA• from a second equivalent of SAM; and (iii) the hydrogen atom abstraction from the methyl group by 5′-dA• (resulting in 5′-dA). Given the parallelism between NifEN-B and RlmN/Cfr in SAM cleavage pattern, NifEN-B (or more specifically, its NifB entity) may utilize a similar methyl transfer mechanism to that used by RlmN and Cfr; only in this case, the methyl group of SAM is used as the carbon source of the interstitial carbide ion. Indeed, incubation of NifEN-B with [methyl-^{14}C] SAM results in the accumulation of ^{14}C label on NifEN-B, suggesting that carbon was incorporated during the K- to L-cluster conversion on this protein [46]. Moreover, the ^{14}C label can then be transferred from NifEN-B to apo NifDK, consistent with the maturation of the newly formed, ^{14}C-labeled L-cluster into an M-cluster and the subsequent delivery of the resultant, ^{14}C-labeled

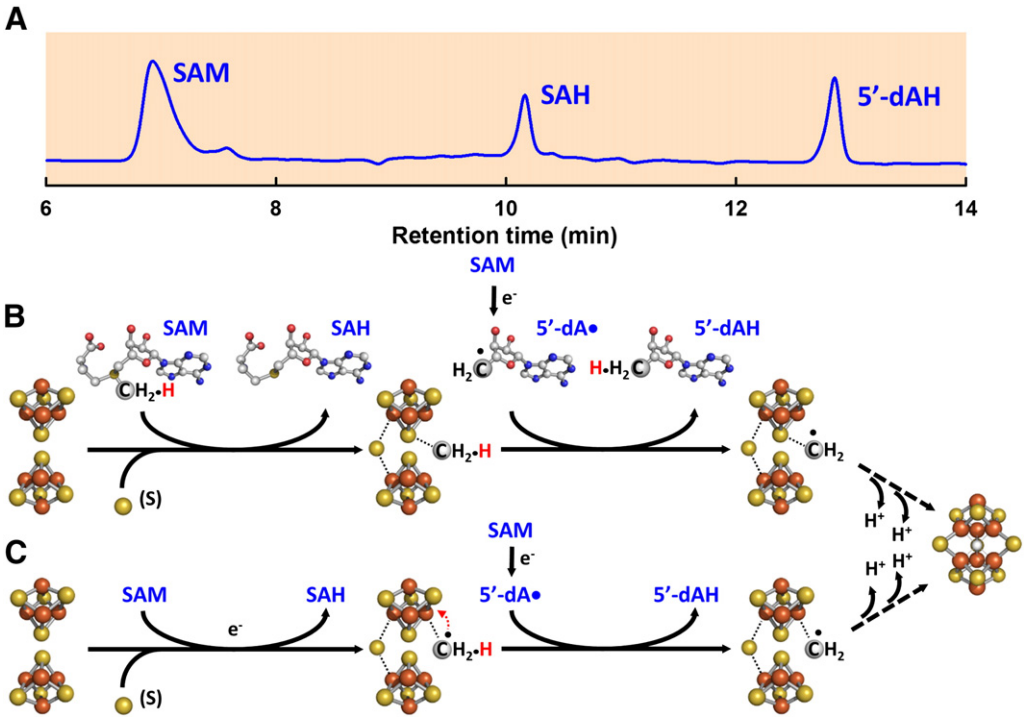

Fig. 6. Cleavage of SAM by NifEN-B (A) and proposed mechanisms of carbon insertion by NifB during L-cluster maturation (B and C). (A) HPLC elution profile of SAM and its cleavage products, SAH and 5′-dA, following the incubation SAM with NifEN-B and dithionite. (B and C) Both carbon insertion mechanisms involve hydrogen atom abstraction from a SAM-derived methyl group, radical-mediated methyl transfer to the K-cluster, and continued deprotonation until an interstitial carbide is formed in the center of the L-cluster. However, the initial step in A involves the transfer of methyl group *via* an SN2 mechanism, followed by the formation of a methylene radical upon hydrogen atom abstraction by 5′-dA• and the subsequent transfer of this radical intermediate to a S atom of the K-cluster; whereas the initial step in B involves the formation of a methyl radical *via* reductive cleavage of SAM, followed by the transfer of this transient intermediate to an Fe atom of the K-cluster and the subsequent processing of this intermediate into a methylene radical. The clusters are shown as ball-and-stick models, with the atoms colored as described in the legend of Fig. 1. PYMOL was used to create the figure (PDB ID: 3PDI).

M-cluster from NifEN-B to apo NifDK [46]. The ^{14}C labels on NifEN-B and NifDK can be traced further to the cluster species (*i.e.*, L- and M-cluster, respectively) rather than the protein peptides [46], suggesting a direct transfer of carbon to the cluster intermediates without going through a protein-bound carbon intermediate step.

It can be postulated, therefore, that a methylene radical is generated through the hydrogen atom abstraction from the methyl group of SAM, which is then transferred to a sulfide atom of K-cluster (Fig. 6B); alternatively, a methyl radical could be generated from SAM, which is then transferred to an iron atom of K-cluster and rearranged into a methylene radical (Fig. 6C). In both scenarios, the carbon intermediate needs to undergo additional deprotonation steps to form a carbide ion. Further, the insertion of carbon must occur concomitantly with the insertion of an additional sulfur atom, as well as the coupling/rearrangement of the two 4Fe units of K-cluster. Together, these processes result in the formation of an L-cluster that already has the interstitial carbide in place (Fig. 6B and C).

3.2. Insertion of Mo and homocitrate

The L-cluster is matured into an M-cluster on NifEN prior to its transfer to NifDK (Fig. 7A and B). Such a conversion can be achieved by an *in vitro* maturation assay, which contains NifH, MgATP, dithionite, molybdate (MoO_4^{2-}) and homocitrate. Upon maturation, a small,

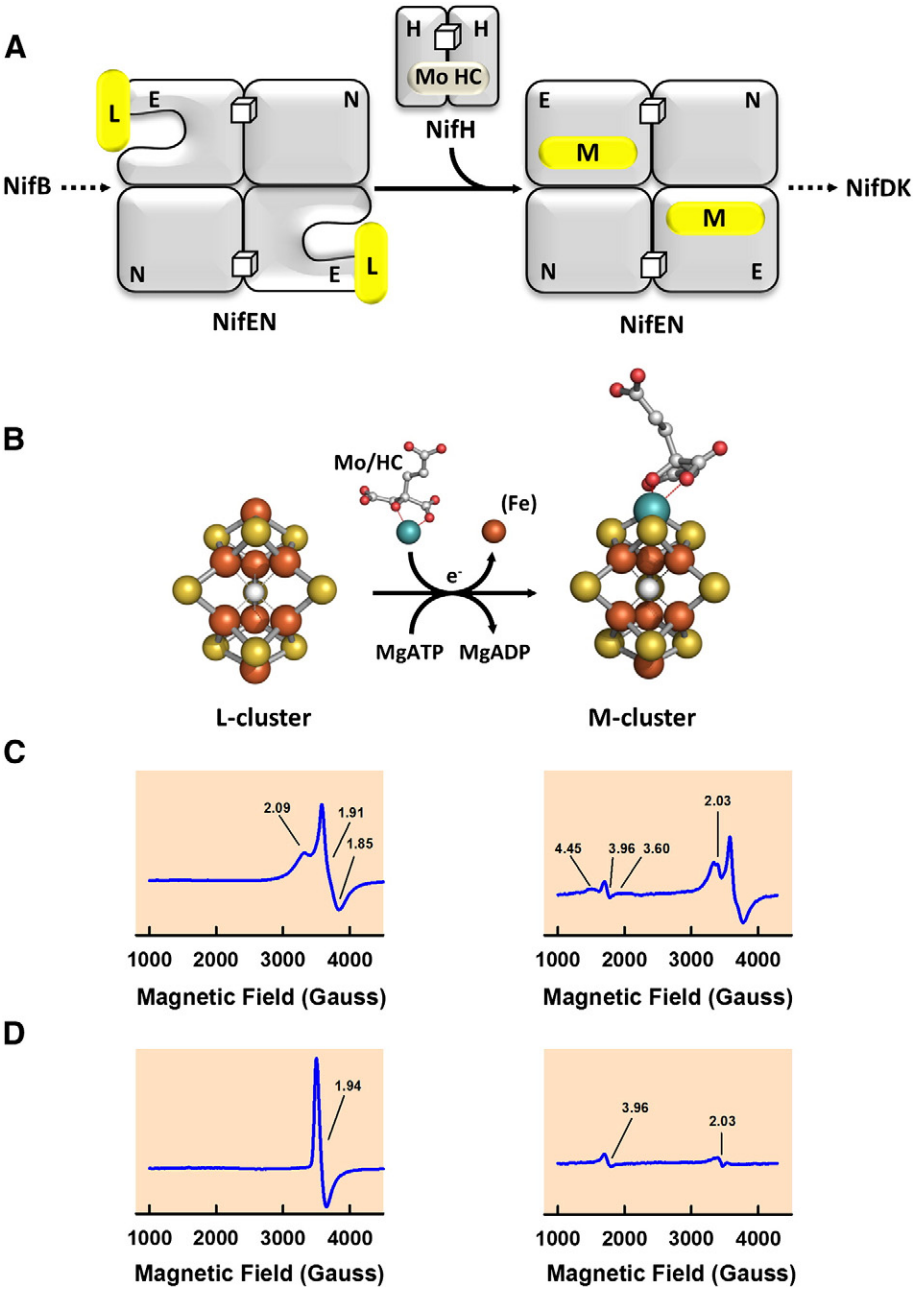

Fig. 7. Schematic presentation (A), structural details (B) and the accompanying spectral changes (C and D) of the formation of M-cluster on NifEN. (A and B) NifEN hosts the conversion of L- to M-cluster upon the replacement of a terminal Fe atom by Mo and homocitrate. NifH serves as an ATP-dependent Mo/homocitrate insertase in this process, and the maturation of L- to M-cluster is likely accompanied by a transfer of the cluster from the surface of NifEN to the M-cluster binding site within the protein. Clusters are shown as ball-and-stick models, with the atoms colored as described in the legend of Fig. 1. PYMOL was used to generate these structures (PDB IDs: 3PDI and 1M1N). (C and D) The L-cluster and the permanent [Fe_4S_4] clusters on NifEN collectively give rise to an $S=1/2$ signal at $g=2.09$, 1.91 and 1.85 in the dithionite-reduced state (C, left); whereas the L-cluster displays a unique $g=1.94$ signal in the IDS-oxidized state (D, left). Upon maturation, the M-cluster on NifEN displays a small signal at $g=4.45$, 3.96, 3.60 and 2.03 in the dithionite-reduced state (C, right); it also displays the $g=3.96$ and 2.03 features of this signal in the IDS-oxidized state (D, right). HC, homocitrate.

M-cluster-like signal appears at $g = 4.45$, 3.96, 3.60 and 2.03 in the spectrum of dithionite-reduced NifEN (Fig. 7C, *right*) concomitant with the decrease of a portion of the $S = 1/2$ signal that corresponds to the L-cluster (Fig. 7C, *left*); whereas the L-cluster-specific, $g = 1.94$ signal (Fig. 7D, *left*) disappears in the spectrum of IDS-oxidized NifEN concomitant with the appearance of the M-cluster-like signal at $g =$ 3.96 and 2.03 (Fig. 7D, *right*). Fe and Mo K-edge XAS/EXAFS analyses [49,50] show that the M-cluster formed on NifEN (Fig. 7B, *right*) is nearly indistinguishable in structure from the M-cluster in NifDK, except for a somewhat asymmetric coordination of Mo that originates from a different ligand environment in NifEN. Maturation of L-cluster cannot occur if ATP is replaced by ADP or non-hydrolyzable ATP analogs, or if the wild-type NifH is replaced by NifH variants that are defective in MgATP hydrolysis [49,50]. Moreover, there is a 3–4 fold increase in maturation efficiency upon a 10 fold increase in dithionite concentration [50]. Since NifH is the only known ATP-dependent reductase in the *in vitro* maturation assay, the ATP- and redox-dependence of L-cluster maturation suggests a crucial role of NifH in this process.

Indeed, NifH re-isolated from the *in vitro* maturation assay is "loaded" with Mo and homocitrate, and it can directly serve as the donor of these two components to the L-cluster on NifEN [51]. Mo K-edge XAS analysis of the loaded NifH reveals a reduction of the number of Mo═O bonds and the effective oxidation state of Mo, which could reflect a change in the formal oxidation state and/or the ligation pattern of Mo. EPR analysis further demonstrates that the loaded NifH displays a signal that is intermediary in line-shape between those of the MgADP- and MgATP-bound forms of NifH [51]. Interestingly, the first structural model of ADP-bound NifH reveals that Mo occupies a position that corresponds to the γ-phosphate of ATP [52]. Given the structural similarity between phosphate and molybdate, the ADP-Mo association could represent the initial step of Mo mobilization by NifH. A binding pattern of NifH/ADP-Mo-homocitrate can be proposed based on these observations, which also reflects the observed co-mobilization of Mo and homocitrate for L-cluster maturation. Moreover, a third role can be proposed for NifH, one in the capacity of an ATP-dependent Mo/homocitrate insertase that enables the maturation of L-cluster on NifEN. Considering the high degree of sequence homology between NifEN and NifDK, NifH may interact with NifEN in an analogous manner to that with NifDK, inducing conformational changes of NifEN that facilitate the "movement" of the cluster species during the maturation process.

Indeed, crystallographic analysis of the L-cluster-bound form of NifEN (designated NifEN) not only confirms the homology in the overall conformations of the two proteins, but also reveals a nearly surface-exposed location of the L-cluster (Fig. 8, *middle*) [45]. In comparison, the M-cluster-bound form of NifDK (designated holo NifDK) has the M-cluster located in a similar location, yet it is buried ~10 Å below the surface of the protein (Fig. 8, *right*). This observation suggests a possible transfer of cluster from the surface to the binding site within NifEN upon maturation, which would be consistent with the sequence-based prediction of an M-cluster binding site that is buried within NifEN. Structural comparison between NifEN and NifDK (Fig. 8, *middle* and *right*) suggests the presence of such an M-cluster binding site beneath the surface of NifEN. Moreover, an analogous cluster transfer mechanism has been proposed for the homologous NifDK. Structural analysis of an M-cluster-deficient form of NifDK (designated apo NifDK) [38] reveals the presence of a positively charged insertion path that extends all the way from the surface to the cluster binding site within NifDK (Fig. 8, *left*), leading to the hypothesis that M-cluster is inserted into NifDK *via* interactions of its negatively charged homocitrate entity with the positively charged

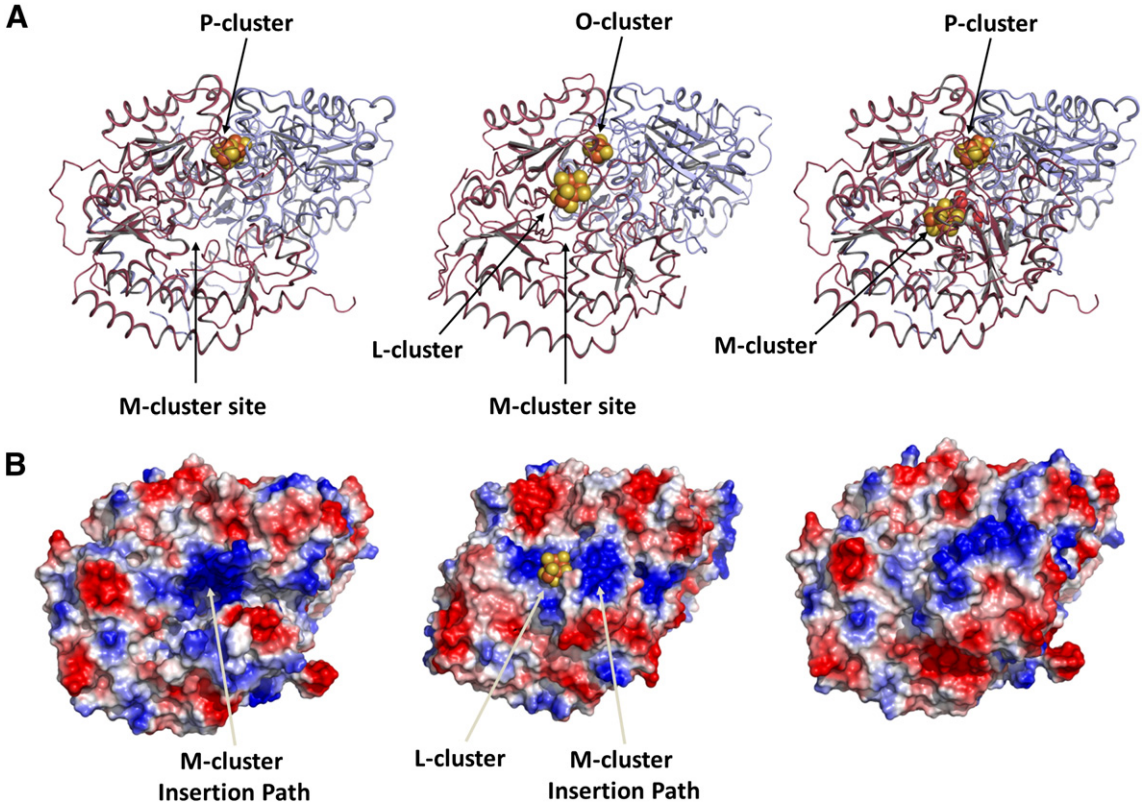

Fig. 8. Ribbon diagrams (A) and surface presentations (B) of apo NifDK, NifEN and holo NifDK. (A) Structures of the αβ-dimers of apo NifDK (left), NifEN (middle), and holo NifDK (right), showing the locations of the Fe/S clusters within these proteins. The permanent $[Fe_4S_4]$ cluster on NifEN (designated O-cluster) is located at the α/β-subunit interface of the protein, and it represents an analog to the permanent $[Fe_8S_7]$ cluster (P-cluster) in NifDK. All clusters are shown as space-filling models, with the atoms colored as described in the legend of Fig. 1. (B) Electrostatic surface potentials of the αβ-dimers of apo-NifDK (left), NifEN (middle) and holo-NifDK (right), showing the locations of insertion funnels in NifDK and NifEN. Negative surface potentials are colored red, while positive surface potentials are colored blue. PYMOL was used to prepare this figure (PDB IDs: 1L5H, 3PDI and 1M1N).

insertion path. Thus, by analogy, the cluster on NifEN could be "relocated" from the surface to the cluster binding site upon maturation. With the assumption that the conformations of apo NifDK and holo NifDK represent the analogous conformations of apo NifEN (L-cluster-deficient) and holo NifEN (M-cluster-bound), NifEN (L-cluster-bound) could very well represent an intermediary assembly snapshot between the two, with the L-cluster "docked" at the entrance of a positively charged funnel and ready to be inserted into its target binding site along this path following the incorporation of Mo and the negatively charged homocitrate (Fig. 8).

3.3. Transfer of M-cluster to its binding site

The M-cluster is delivered from its binding site in NifEN to its binding site in NifDK *via* direct protein–protein interactions [49]. Such a direct transfer mechanism is supported by the observation that holo NifEN (M-cluster-bound) can form a complex with apo NifDK, which subsequently leads to the reconstitution and activation of apo NifDK. In contrast, NifEN (L-cluster-bound) is unable to complex with and activate apo NifDK, suggesting that the L- to M-cluster conversion on NifEN triggers the docking of NifEN on NifDK and the subsequent transfer of M-cluster from the former to the latter [53]. Interestingly, the incorporation of Mo alone into the L-cluster is sufficient to induce a conformational change that is required for the complex formation between NifEN and apo NifDK. However, this homocitrate-free cluster cannot be transferred to NifDK, suggesting that the negatively charged homocitrate entity is crucial for the insertion of M-cluster into NifDK [53]. Sequence comparison between NifEN and NifDK reveals that certain residues of NifDK that either provide a covalent ligand to the M-cluster or tightly pack the M-cluster within the polypeptide matrix are not duplicated in the sequence of NifEN [40]. It is possible, therefore, that the M-cluster binding sites in NifEN and NifDK are brought in close proximity upon complex formation between the two proteins, which facilitates the subsequent "diffusion" of M-cluster from its transient binding site in NifEN ("low affinity site") to its targe binding site in NifDK ("high affinity site").

Based on the structural comparison between apo NifDK, NifEN and holo NifDK (Fig. 8), a common pathway of cluster insertion can be proposed for NifEN and NifDK, which involves the formation of an apo protein with an open insertion funnel, the docking of the cluster at the entrance of the funnel, and the subsequent insertion of the cluster into the funnel (Fig. 9A). The two pathways are linked by the interactions between NifEN and NifDK, which result in a conformational change of NifEN that facilitates the release of M-cluster from its

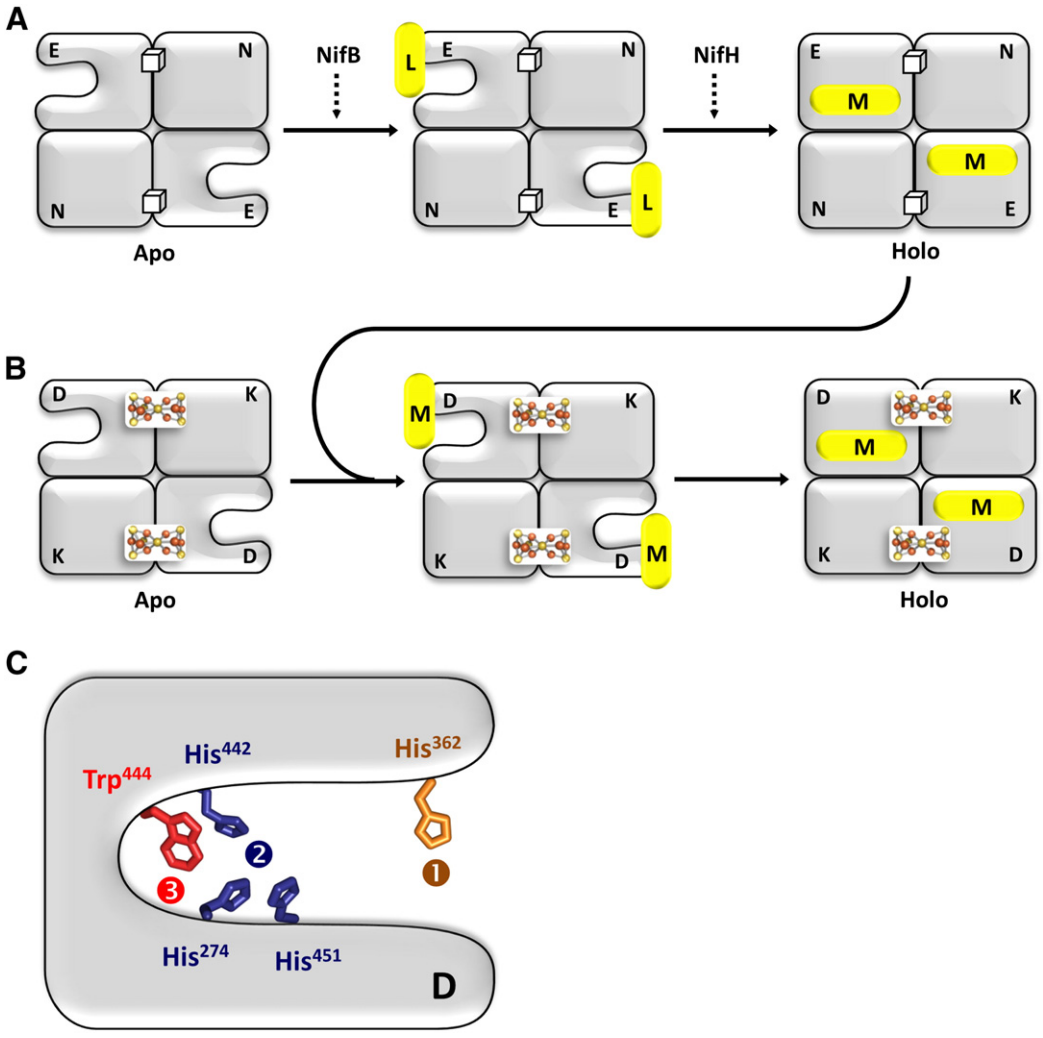

Fig. 9. Transfer of M-cluster between NifEN and NifDK (A and B) and the insertion funnel of M-cluster within NifDK (C). (A and B) NifEN and NifDK share a common cluster insertion mechanism, which involves the formation of an apo protein with an insertion funnel, the docking of the cluster at the entrance of the funnel, and the subsequent insertion of the cluster into the funnel. The biosynthetic events on NifEN and NifDK are connected *via* complex formation and cluster transfer between the two proteins. The permanent [Fe_4S_4] clusters (or O-clusters) on NifEN are depicted as white cubes, while the permanent [Fe_8S_7] P-clusters on NifDK are depicted as ball-and-stick models in grey ovals. Transient clusters are indicated as yellow ovals. (C) Schematic presentation of the M-cluster insertion funnel in the α-subunit of apo NifDK, showing ① the "lid loop" residue, $His^{\alpha 362}$ (orange); ② the "His triad" residues, $His^{\alpha 274}$, $His^{\alpha 442}$ and $His^{\alpha 451}$ (dark blue); and ③ the "switch/lock" residues, $His^{\alpha 442}$ and $Trp^{\alpha 444}$ (red). The residues are shown as sticks.

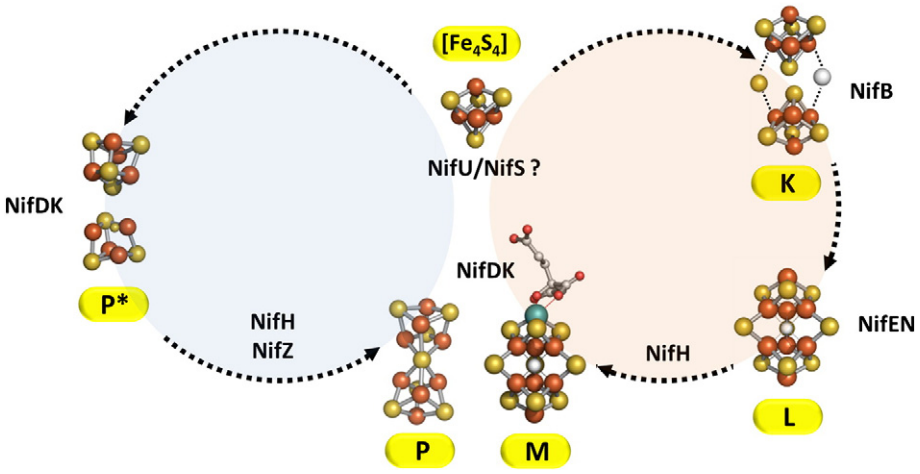

Fig. 10. Flow diagrams of the biosynthetic pathways of P-cluster (blue circle) and M-cluster (red circle). The assembly pathways of both P- and M-clusters presumably start with the combined action of NifS and NifU, which generates [Fe_4S_4] units as building blocks for these clusters. The coupling of a pair of [Fe_4S_4]-like modules (P*-cluster) on NifDK requires the participation of NifH and NifZ, and it results in the formation of an [Fe_8S_7] P-cluster; whereas the fusion of two [Fe_4S_4] modules (K-cluster) on NifB relies on radical SAM chemistry, and it involves the insertion of C and S atoms concomitant with the formation of an [Fe_8S_9] L-cluster. The L-cluster is further processed on NifEN into a [$MoFe_7S_9C$-homocitrate] M-cluster upon NifH-mediated insertion of Mo and homocitrate. All clusters are shown as ball-and-stick models, with the atoms colored as described in the legend of Fig. 1. PYMOL was used to create the figure (PDB IDs: 1M1N and 3PDI).

transient binding site back to the surface of NifEN. Subsequently, the M-cluster is "deposited" onto the surface of NifDK, likely through the coordinated actions of cysteinyl ligands, such as the $Cys^{\alpha 25}$ in NifEN and the corresponding $Cys^{\alpha 45}$ in NifDK, which enable an efficient intermolecular transfer of M-cluster while preventing the escape of the cluster into the surrounding environment.

Once delivered to the surface of NifDK, the M-cluster interacts with a number of NifDK residues *en route* to its target binding site. Located in three key regions along the insertion path in apo NifDK (Fig. 9B), these residues include: (i) the "lid loop" residues (*i.e.*, α353 to α364, with $His^{\alpha 362}$ located at the "tip" of the loop), which could serve as transient ligand(s) for the M-cluster at the entrance of the insertion path; (ii) the "His triad" residues (*i.e.*, $His^{\alpha 274}$, $His^{\alpha 442}$ and $His^{\alpha 451}$), which could provide a docking point for the M-cluster halfway down the path; and (iii) the "switch/lock" residues (*i.e.*, $His^{\alpha 442}$ and $Trp^{\alpha 444}$), which could secure the M-cluster at its binding site *via* the bulky side chain of $Trp^{\alpha 444}$ once it switches positions with $His^{\alpha 442}$ [38]. Mutational analyses provide support to the proposed roles of these residues, showing a specific and significant decrease in the level of M-cluster incorporation upon removal of the positive charge, the ligand capacity and the steric effect at these positions [54–56]. Small angle x-ray scattering (SAXS) analyses further demonstrate that apo NifDK ($R_g = 42.4$ Å) is more extended in conformation than holo NIfDK ($R_g = 40.2$ Å), suggesting that the insertion of M-cluster has a "compacting" effect on the overall conformation of NifDK [34].

4. Summary

There is a certain degree of parallelism between the biosynthetic pathways of P- and M-clusters (Fig. 10). Both utilize paired 4Fe units as building blocks, and both involve the fusion of two 4Fe modules into an 8Fe cluster. These similarities render a topological resemblance between the two clusters, which is illustrated by the successful chemical synthesis of P- and M-cluster topologs *via* the rearrangement of similar core structures [57,58]. On the other hand, the assembly of M-cluster also involves the insertion of additional elements (*i.e.*, S and C), the rearrangement of "equatorial" Fe atoms, and the substitution of one apical Fe for Mo and homocitrate. These extra processing steps may account for the more elaborate, *ex situ* synthetic route taken by the M-cluster. Further investigations of P- and M-cluster biosynthesis are currently underway, which will hopefully provide new chemical insights into the structure and function of nitrogenase.

Acknowledgement

This work was supported by National Institutes of Health grant GM-67626 (M.W.R.).

References

[1] B.K. Burgess, D.J. Lowe, Mechanism of molybdenum nitrogenase, Chem. Rev. 96 (1996) 2983–3012.
[2] J.B. Howard, D.C. Rees, Structural basis of biological nitrogen fixation, Chem. Rev. 96 (1996) 2965–2982.
[3] R.D. Joerger, P.E. Bishop, Bacterial alternative nitrogen fixation systems, Crit. Rev. Microbiol. 16 (1988) 1–14.
[4] O. Einsle, F.A. Tezcan, S.L. Andrade, B. Schmid, M. Yoshida, J.B. Howard, D.C. Rees, Nitrogenase MoFe-protein at 1.16 Å resolution: a central ligand in the FeMo-cofactor, Science 297 (2002) 1696–1700.
[5] J. Kim, D.C. Rees, Crystallographic structure and functional implications of the nitrogenase molybdenum iron protein from *Azotobacter vinelandii*, Nature 360 (1992) 553–560.
[6] K.M. Lancaster, M. Roemelt, P. Ettenhuber, Y. Hu, M.W. Ribbe, F. Neese, U. Bergmann, S. DeBeer, X-ray emission spectroscopy evidences a central carbon in the nitrogenase iron-molybdenum cofactor, Science 334 (2011) 974–977.
[7] T. Spatzal, M. Aksoyoglu, L. Zhang, S.L. Andrade, E. Schleicher, S. Weber, D.C. Rees, O. Einsle, Evidence for interstitial carbon in nitrogenase FeMo cofactor, Science 334 (2011) 940.
[8] H. Schindelin, C. Kisker, J.L. Schlessman, J.B. Howard, D.C. Rees, Structure of ADP•AlF4$^-$-stabilized nitrogenase complex and its implications for signal transduction, Nature 387 (1997) 370–376.
[9] A.J. Pierik, H. Wassink, H. Haaker, W.R. Hagen, Redox properties and EPR spectroscopy of the P-clusters of *Azotobacter vinelandii* MoFe protein, Eur. J. Biochem. 212 (1993) 51–61.
[10] K.K. Surerus, M.P. Hendrich, P.D. Christie, D. Rottgardt, W.H. Orme-Johnson, E. Münck, Mössbauer and integer-spin EPR of the oxidized P-clusters of nitrogenase — P^{ox} is a non-kramers system with a nearly degenerate ground doublet, J. Am. Chem. Soc. 114 (1992) 8579–8590.
[11] G.D. Watt, A. Burns, S. Lough, D.L. Tennent, Redox and spectroscopic properties of oxidized MoFe protein from *Azotobacter vinelandii*, Biochemistry 19 (1980) 4926–4932.
[12] M.K. Chan, J. Kim, D.C. Rees, The nitrogenase FeMo-cofactor and P-cluster pair: 2.2 Å resolution structures, Science 260 (1993) 792–794.
[13] J.W. Peters, M.H. Stowell, S.M. Soltis, M.G. Finnegan, M.K. Johnson, D.C. Rees, Redox-dependent structural changes in the nitrogenase P-cluster, Biochemistry 36 (1997) 1181–1187.
[14] B.K. Burgess, The iron molybdenum cofactor of nitrogenase, Chem. Rev. 90 (1990) 1377–1406.
[15] J.B. Howard, D.C. Rees, How many metals does it take to fix N_2? A mechanistic overview of biological nitrogen fixation, Proc. Natl. Acad. Sci. U. S. A. 103 (2006) 17088–17093.
[16] V.K. Shah, W.J. Brill, Isolation of an iron–molybdenum cofactor from nitrogenase, Proc. Natl. Acad. Sci. U. S. A. 74 (1977) 3249–3253.
[17] A.W. Fay, M.A. Blank, C.C. Lee, Y, Hu, K.O. Hodgson, B. Hedman, M.W. Ribbe, Characterization of isolated nitrogenase FeVco, J. Am. Chem. Soc. 132 (2010) 12612–12618.
[18] H.-I. Lee, B.J. Hales, B.M. Hoffman, Metal-ion valencies of the FeMo cofactor in CO-inhibited and resting state nitrogenase by Fe-57 Q-band ENDOR, J. Am. Chem. Soc. 119 (1997) 11395–11400.

[19] S.J. Yoo, H.C. Angove, V. Papaefthymiou, B.K. Burgess, E. Münck, Mössbauer study of the MoFe protein of nitrogenase from *Azotobacter vinelandii* using selective Fe^{57} enrichment of the M-centers, J. Am. Chem. Soc. 122 (2000) 4926–4936.
[20] L.M. Rubio, P.W. Ludden, Biosynthesis of the iron–molybdenum cofactor of nitrogenase, Annu. Rev. Microbiol. 62 (2008) 93–111.
[21] S.C. Lee, R.H. Holm, The clusters of nitrogenase: synthetic methodology in the construction of weak-field clusters, Chem. Rev. 104 (2004) 1135–1158.
[22] M.L. Hlavinka, T. Miyaji, R.J. Staples, R.H. Holm, Hydroxide-promoted core conversions of molybdenum-iron-sulfur edge-bridged double cubanes: Oxygen-ligated topological P^N clusters, Inorg. Chem. 46 (2007) 9192–9200.
[23] Y. Ohki, M. Imada, A. Murata, Y. Sunada, S. Ohta, M. Honda, T. Sasamori, N. Tokitoh, M. Katada, K. Tatsumi, Synthesis, structures, and electronic properties of [8Fe-7S] cluster complexes modeling the nitrogenase P-cluster, J. Am. Chem. Soc. 131 (2009) 13168–13178.
[24] Y. Ohki, Y. Sunada, M. Honda, M. Katada, K. Tatsumi, Synthesis of the P-cluster inorganic core of nitrogenases, J. Am. Chem. Soc. 125 (2003) 4052–4053.
[25] Y. Zhang, R.H. Holm, Structural conversions of molybdenum-iron-sulfur edge-bridged double cubanes and P^N-type clusters topologically related to the nitrogenase P-cluster, Inorg. Chem. 43 (2004) 674–682.
[26] Y. Zhang, J.L. Zuo, H.C. Zhou, R.H. Holm, Rearrangement of symmetrical dicubane clusters into topological analogues of the P cluster of nitrogenase: nature's choice? J. Am. Chem. Soc. 124 (2002) 14292–14293.
[27] Y. Ohki, K. Tanifuji, N. Yamada, R.E. Cramer, K. Tatsumi, Formation of a nitrogenase P-cluster [Fe_8S_7] core *via* reductive fusion of two all-ferric [Fe_4S_4] clusters, Chem. Asian J. 7 (2012) 2222–2224.
[28] M.W. Ribbe, Y. Hu, M. Guo, B. Schmid, B.K. Burgess, The FeMoco-deficient MoFe protein produced by a *nifH*-deletion strain of *Azotobacter vinelandii* shows unusual P-cluster features, J. Biol. Chem. 277 (2002) 23469–23476.
[29] M.C. Corbett, Y. Hu, F. Naderi, M.W. Ribbe, B. Hedman, K.O. Hodgson, Comparison of iron-molybdenum cofactor deficient nitrogenase MoFe proteins by X-ray absorption spectroscopy: Implications for P-cluster biosynthesis, J. Biol. Chem. 279 (2004) 28276–28282.
[30] C.C. Lee, M.A. Blank, A.W. Fay, J.M. Yoshizawa, Y. Hu, K.O. Hodgson, B. Hedman, M.W. Ribbe, Stepwise formation of P-cluster in nitrogenase MoFe protein, Proc. Natl. Acad. Sci. U. S. A. 106 (2009) 18474–18478.
[31] R.B. Broach, K. Rupnik, Y. Hu, A.W. Fay, M. Cotton, M.W. Ribbe, B.J. Hales, VTVH-MCD spectroscopic study of the metal clusters in the Δ*nifB* and Δ*nifH* MoFe proteins of nitrogenase from *Azotobacter vinelandii*, Biochemistry 45 (2006) 15039–15048.
[32] K. Rupnik, C.C. Lee, Y. Hu, M.W. Ribbe, B.J. Hales, $[4Fe4S]^{2+}$ clusters exhibit ground-state paramagnetism, J. Am. Chem. Soc. 133 (2011) 6871–6873.
[33] A.D. Smith, G.N.L. Jameson, P.C. Dos Santos, J.N. Agar, S. Naik, C. Krebs, J. Frazzon, D.R. Dean, B.H. Huynh, M.K. Johnson, NifS-mediated assembly of [4Fe-4S] clusters in the N- and C-terminal domains of the NifU scaffold protein, Biochemistry 44 (2005) 12955–12969.
[34] M.C. Corbett, Y. Hu, A.W. Fay, H. Tsuruta, M.W. Ribbe, K.O. Hodgson, B. Hedman, Conformational differences between *Azotobacter vinelandii* nitrogenase MoFe proteins as studied by small angle X-ray scattering, Biochemistry 46 (2007) 8066–8074.
[35] Y. Hu, A.W. Fay, P.C. Dos Santos, F. Naderi, M.W. Ribbe, Characterization of *Azotobacter vinelandii nifZ* deletion strains - Indication of stepwise MoFe protein assembly, J. Biol. Chem. 279 (2004) 54963–54971.
[36] M.S. Cotton, K. Rupnik, R.B. Broach, Y. Hu, A.W. Fay, M.W. Ribbe, B.J. Hales, VTVH-MCD study of the Δ*nifB*Δ*nifZ* MoFe protein from *Azotobacter vinelandii*, J. Am. Chem. Soc. 131 (2009) 4558–4559.
[37] Y. Hu, A.W. Fay, C.C. Lee, M.W. Ribbe, P-cluster maturation on nitrogenase MoFe protein, Proc. Natl. Acad. Sci. U. S. A. 104 (2007) 10424–10429.
[38] B. Schmid, M.W. Ribbe, O. Einsle, M. Yoshida, L.M. Thomas, D.R. Dean, D.C. Rees, B.K. Burgess, Structure of a cofactor-deficient nitrogenase MoFe protein, Science 296 (2002) 352–356.
[39] R.M. Allen, R. Chatterjee, P.W. Ludden, V.K. Shah, Incorporation of iron and sulfur from NifB cofactor into the iron-molybdenum cofactor of dinitrogenase, J. Biol. Chem. 270 (1995) 26890–26896.
[40] G. Schwarz, R.R. Mendel, M.W. Ribbe, Molybdenum cofactors, enzymes and pathways, Nature 460 (2009) 839–847.
[41] J.A. Wiig, Y. Hu, M.W. Ribbe, NifEN-B complex of *Azotobacter vinelandii* is fully functional in nitrogenase FeMo cofactor assembly, Proc. Natl. Acad. Sci. U. S. A. 108 (2011) 8623–8627.
[42] M.C. Corbett, Y. Hu, A.W. Fay, M.W. Ribbe, B. Hedman, K.O. Hodgson, Structural insights into a protein-bound iron-molybdenum cofactor precursor, Proc. Natl. Acad. Sci. U. S. A. 103 (2006) 1238–1243.
[43] A.W. Fay, M.A. Blank, C.C. Lee, Y. Hu, K.O. Hodgson, B. Hedman, M.W. Ribbe, Spectroscopic characterization of the isolated iron-molybdenum cofactor (FeMoco) precursor from the protein NifEN, Angew. Chem. Int. Ed Engl. 50 (2011) 7787–7790.
[44] Y. Hu, A.W. Fay, M.W. Ribbe, Identification of a nitrogenase iron-molybdenum cofactor precursor on NifEN complex, Proc. Natl. Acad. Sci. U. S. A. 102 (2005) 3236–3241.
[45] J.T. Kaiser, Y. Hu, J.A. Wiig, D.C. Rees, M.W. Ribbe, Structure of precursor-bound NifEN: A nitrogenase FeMo cofactor maturase/insertase, Science 331 (2011) 91–94.
[46] J.A. Wiig, Y. Hu, C.C. Lee, M.W. Ribbe, Radical SAM-dependent carbon insertion into nitrogenase M-cluster, Science 337 (2012) 1672–1675.
[47] T.L. Grove, J.S. Benner, M.I. Radle, J.H. Ahlum, B.J. Landgraf, C. Krebs, S.J. Booker, A radically different mechanism for S-adenosylmethionine-dependent methyltransferases, Science 332 (2011) 604–607.
[48] A.K. Boal, T.L. Grove, M.I. McLaughlin, N.H. Yennawar, S.J. Booker, A.C. Rosenzweig, Structural basis for methyl transfer by a radical SAM enzyme, Science 332 (2011) 1089–1092.
[49] Y. Hu, M.C. Corbett, A.W. Fay, J.A. Webber, K.O. Hodgson, B. Hedman, M.W. Ribbe, FeMo cofactor maturation on NifEN, Proc. Natl. Acad. Sci. U. S. A. 103 (2006) 17119–17124.
[50] J.M. Yoshizawa, M.A. Blank, A.W. Fay, C.C. Lee, J.A. Wiig, Y. Hu, K.O. Hodgson, B. Hedman, M.W. Ribbe, Optimization of FeMoco Maturation on NifEN, J. Am. Chem. Soc. 131 (2009) 9321–9325.
[51] Y. Hu, M.C. Corbett, A.W. Fay, J.A. Webber, K.O. Hodgson, B. Hedman, M.W. Ribbe, Nitrogenase Fe protein: A moybdate/homocitrateinsertase, Proc. Natl. Acad. Sci. U. S. A. 103 (2006) 17125–17130.
[52] M.M. Georgiadis, H. Komiya, P. Chakrabarti, D. Woo, J.J. Kornuc, D.C. Rees, Crystallographic structure of the nitrogenase iron protein from *Azotobacter vinelandii*, Science 257 (1992) 1653–1659.
[53] A.W. Fay, M.A. Blank, J.M. Yoshizawa, C.C. Lee, J.A. Wiig, Y. Hu, K.O. Hodgson, B. Hedman, M.W. Ribbe, Formation of a homocitrate-free iron-molybdenum cluster on NifEN: Implications for the role of homocitrate in nitrogenase assembly, Dalton Trans. 39 (2010) 3124–3130.
[54] A.W. Fay, Y. Hu, B. Schmid, M.W. Ribbe, Molecular insights into nitrogenase FeMoco insertion – The role of His 274 and His 451 of MoFe protein α subunit, J. Inorg. Biochem. 101 (2007) 1630–1641.
[55] Y. Hu, A.W. Fay, M.W. Ribbe, Molecular insights into nitrogenase FeMoco insertion – The role of His362 of MoFe protein α subunit in FeMoco incorporation, J. Biol. Inorg. Chem. 12 (2007) 449–460.
[56] Y. Hu, A.W. Fay, B. Schmid, B. Makar, M.W. Ribbe, Molecular insights into nitrogenase FeMoco insertion - Trp 444 of MoFe protein α subunit locks FeMoco in its binding site, J. Biol. Chem. 281 (2006) 30534–30541.
[57] Y. Ohki, Y. Ikagawa, K. Tatsumi, Synthesis of new [8Fe-7S] clusters: a topological link between the core structures of P-cluster, FeMo-co, and FeFe-co of nitrogenases, J. Am. Chem. Soc. 129 (2007) 10457–10465.
[58] Y. Zhang, R.H. Holm, Synthesis of a molecular $Mo_2Fe_6S_9$ cluster with the topology of the P^N cluster of nitrogenase by rearrangement of an edge-bridged $Mo_2Fe_6S_8$ double cubane, J. Am. Chem. Soc. 125 (2003) 3910–3920.
[59] G. Palmer, Electronic paramagnetic resonance of metalloproteins, in: L. Que Jr. (Ed.), Physical Methods in Bioinorganic Chemistry: Spectroscopy and Magnetism, University Science Books, Sausalito, California, 2000, pp. 121–185.
[60] R.A. Scott, X-ray absorption spectroscopy, in: L. Que Jr. (Ed.), Physical Methods in Bioinorganic Chemistry: Spectroscopy and Magnetism, University Science Books, Sausalito, California, 2000, pp. 465–503.